Eur. Phys. J. D **7**, 269–278 (1999)

THE EUROPEAN PHYSICAL JOURNAL D

EDP Sciences

Semi-classical theory of laser cooling in two dimensions

H. Pu, T. Cai, and N.P. Bigelow[a]

Department of Physics and Astronomy, Laboratory for Laser Energetics, University of Rochester, Rochester, New York 14627, USA

Received 4 December 1998 and Received in final form 13 February 1999

Abstract. We present a semi-classical theory of the light pressure force for atoms interacting with a two-dimensional laser field. Unlike previous 2D theory, ours is valid for general atomic level and laser field configurations. We show that striking new features appear in the velocity-dependent force arising from the multi-dimensionality. Finally, we describe in detail the novel numerical technique used in the calculation.

PACS. 32.80.Pj Optical cooling of atoms; trapping

1 Introduction

The possibility of cooling atoms with laser light was first proposed by Hänsch and Schawlow [1], and also by Wineland and Dehmelt [2], in 1975: due to the Doppler effect, a two-level atom moving in a region of counter-propagating laser beams will scatter more photons from the beam opposing the motion if the laser is tuned to the low frequency side of the atomic resonance. A more rigorous theory of this Doppler cooling was later developed by Minogin and Letokhov, by Kazantsev and by Stenholm [3]. In the early 80's, Gordon and Ashkin [4] calculated the force exerted on a two-level atom by laser light and discussed in detail the idea of momentum diffusion, showing how the cooling from the light pressure force and the heating from diffusion balance each other and drive the system to an equilibrium.

Laser cooling in three dimension was first demonstrated in the AT&T Bell Laboratories in 1985 [5], and the temperature measured agreed well with the prediction of the simple 1D Doppler theory. But three years later, a group at NIST [6] measured sample temperatures an order of magnitude below the limit of the Doppler theory. This discovery prompted a reexamination of laser cooling theory, focusing on the multilevel nature of the real atoms used in the experiment. Before long, polarization gradient cooling was proposed by Dalibard and Cohen-Tannoudji at École Normale Superieure [7], and Chu *et al.* at Stanford [8]. This cooling mechanism depends on the interplay of effects such as optical pumping, light shifts and the motion of atoms in light fields with polarization gradients.

All the above mentioned theories treat an atom interacting with a *one*-dimensional light field. For more than one spatial dimension, however, the picture still remains incomplete. This limitation is particularly significant given that most existing experiments deal with inherently multi-dimensional systems. Indeed, many intriguing phenomena have been observed which cannot be well explained by the one-dimensional theories.

Several efforts have been made to analyze the light pressure force and atomic momentum distribution in more than one dimension. Particular attention has been paid to the case of a two-level atom interacting with a two-dimensional light field. In 1989, Kazantsev and Krasnov pointed out that such an atom can experience a spontaneous force with vortex structure [9]. Hemmerich and Hänsch reported some experimental observations of rubidium atoms interacting with a two-dimensional laser field [10]. Their experiments confirmed the prediction of the theoretical model that the atomic motion depends strongly on the time-phase delay φ between the two orthogonal standing waves. Mølmer *et al.* have studied both two-level and multi-level atoms interacting with two-dimensional light fields [11]. They also predicted that the force is φ-dependent, an effect confirmed by the Monte-Carlo simulations. Finkelstein *et al.* [12] and Castin *et al.* [13] have investigated the interaction of a $J_{\rm g} = 1/2$ atom ($J_{\rm g}$ being the ground state angular momentum quantum number) with a particular 2D laser configuration (two orthogonal standing waves propagating at x, y axes and polarized at y and x directions, respectively). They found that the light pressure force is not isotropic for certain values of φ and that this may result in velocity space channeling along certain directions. Similar behavior was also found by Cai and Bigelow who calculated the 2D velocity-dependent force on both two and three-level atoms [14].

All these results tell us that there are qualitatively different features for an atom interacting with a 2D light fields as compared to its interaction with a comparable 1D field. However, there remain significant limitations to the results obtained: some treat the atom as a two-level system, which may often be an oversimplified approximation of reality; some carry out numerical simulations based on Monte-Carlo methods which provide some insights but may obscure the essence of the atom-field

[a] e-mail: nbig@lle.rochester.edu

interactions; some calculations neglect the excited state populations and ground-excited coherence, an approximation only valid for weak field strength or large detunings, and low atomic velocities. To overcome some of these limitations, we present here a semi-classical theory of the mechanical effects of a 2D laser field on an atom. Our technique is based on a Floquet approach in which we use a matrix generalization [15] of the continued fraction procedure to solve the optical Bloch equations. Using this theory, we are able to calculate the velocity-dependent light pressure forces (i) for an arbitrary $J_g \leftrightarrow J_e$ electric dipole transition ($|J_e - J_g| = 0, \pm 1$); (ii) for an arbitrary 2D laser field configuration; (iii) with or without the presence of magnetic fields; (iv) including all the internal atomic states and the coherences between them, which makes our calculations applicable to both weak and strongly saturating laser field strengths with arbitrary detunings. Using the same technique, we can also calculate the momentum diffusion tensor. Together with the light pressure force, we are therefore able to study the atomic distribution in momentum space by solving the Fokker-Planck equation.

In Section 2, we describe the procedures to calculate the 2D light pressure force and to solve the Fokker-Planck equation. The detailed technique of 2D continued fraction method is presented in the Appendix. In Section 3, we apply our theory to study a multi-level atom with $J_g = 1 \leftrightarrow J_e = 1$ dipole transition interacting with a 2D laser field with $\sigma^+ - \sigma_-$ configuration, which corresponds to the experimental situation of the 2D VSCPT configuration investigated by Lawall *et al.* [16].

2 Basic formalism

The theory presented here is a semi-classical one. It is valid under the assumptions that: (1) the natural linewidth of the atomic excited state is much larger than the recoil energy, *i.e.*, $\hbar\Gamma \gg \hbar^2k^2/2m$, where Γ, k and m are the excited state spontaneous emission rate, wave number of the light field and atomic mass, respectively; and (2) the atomic momentum distribution width is much greater than the single photon recoil momentum, *i.e.*, $\Delta p \gg \hbar k$.

The system under consideration is a multi-level atom with $J_g \leftrightarrow J_e$ dipole transition interacting with a monochromatic 2D light wave with frequency ω_L. The electric field can be described using the following general expression:

$$\mathbf{E}(\mathbf{r}) = \sum_{q=0,\pm1} E_q(\mathbf{r})\hat{\mathbf{e}}_q^z \mathrm{e}^{-\mathrm{i}\omega_L t} + cc \tag{1}$$

where $\hat{\mathbf{e}}_0^z = \hat{\mathbf{e}}_z$, $\hat{\mathbf{e}}_{\pm1}^z = \mp(\hat{\mathbf{e}}_x \pm \mathrm{i}\hat{\mathbf{e}}_y)/\sqrt{2}$. The ground and excited state sublevels form two Zeeman multiplets:

$$\begin{aligned} \hat{J}_z|g_{m_g}\rangle &= m_g\hbar|g_{m_g}\rangle, \\ m_g &= -J_g, -J_g+1, \cdots, J_g-1, J_g, \\ \hat{J}_z|e_{m_e}\rangle &= m_e\hbar|e_{m_e}\rangle, \\ m_e &= -J_e, -J_e+1, \cdots, J_e-1, J_g. \end{aligned} \tag{2}$$

Assuming that a static magnetic field $B\hat{\mathbf{e}}_z$ is present, the direction of which, without loss of generality, has been chosen to be in the z-direction, the atomic Hamiltonian $\hat{H}_A$ then reads:

$$\begin{aligned} \hat{H}_A = \frac{\hat{P}^2}{2m} &- \hbar \sum_{m_e=-J_e}^{J_e} \left(\frac{\Delta}{2} + \omega_B m_e g_e\right) |e_{m_e}\rangle\langle e_{m_e}| \\ &- \hbar \sum_{m_g=-J_g}^{J_g} \left(-\frac{\Delta}{2} + \omega_B m_g g_g\right) |g_{m_g}\rangle\langle g_{m_g}| \end{aligned} \tag{3}$$

where $\Delta \equiv \omega_L - \omega_A$ is the laser detuning with respect to the atomic transition in free space, $\omega_B \equiv \mu B/\hbar$ is the Larmor frequency, with μ being the atomic magnetic dipole moment and g_g, g_e are Landé g-factors for the ground and excited state, respectively. Under the rotation wave approximation, the atom-laser interaction Hamiltonian $\hat{H}_{A-L} = -\hat{\mathbf{D}}\cdot\mathbf{E}$ reads:

$$\begin{aligned} \hat{H}_{A-L} = -\frac{\hbar}{2} &\sum_{m_g=-J_g}^{J_g} \sum_{q=0,\pm1} \langle J_g, m_g, 1, q | J_e, m_g + q\rangle \\ &\times g_q(\mathbf{r})|e_{m_g+q}\rangle\langle g_{m_g}| + h.c. \end{aligned} \tag{4}$$

where $\langle j_1, m_1, j_2, m_2|j, m\rangle$ are Clebsch-Gordan coefficients for dipole transitions and we have defined the complex Rabi frequencies $g_q(\mathbf{r})$:

$$g_q(\mathbf{r}) = \frac{2\langle e\|d\|g\rangle E_q(\mathbf{r})}{\hbar}, \quad q = 0, \pm1 \tag{5}$$

with $\langle e\|d\|g\rangle$ being the electric dipole moment between the ground and excited state.

The evolution of the atomic density operator is governed by the optical Bloch equation:

$$\frac{\mathrm{d}\hat{\rho}}{\mathrm{d}t} = \frac{1}{\mathrm{i}\hbar}[\hat{H}_A + \hat{H}_{A-L},\, \hat{\rho}] + S(\hat{\rho}) \tag{6}$$

where $S(\hat{\rho})$ represents terms accounting for spontaneous emission arising from the atom-vacuum coupling [17]:

$$\begin{aligned} S(\hat{\rho}) = -\frac{\Gamma}{2}&[(\hat{\mathbf{S}}_+\cdot\hat{\mathbf{S}}_-)\hat{\rho} + \hat{\rho}(\hat{\mathbf{S}}_+\cdot\hat{\mathbf{S}}_-)] \\ &+\Gamma\int \frac{\mathrm{d}^2\kappa}{8\pi/3} \sum_{\boldsymbol{\varepsilon}\perp\boldsymbol{\kappa}} (\hat{\mathbf{S}}_-\cdot\boldsymbol{\varepsilon}^*)[\mathrm{e}^{-\mathrm{i}\boldsymbol{\kappa}\cdot\mathbf{r}}\hat{\rho}\mathrm{e}^{\mathrm{i}\boldsymbol{\kappa}\cdot\mathbf{r}}](\hat{\mathbf{S}}_+\cdot\boldsymbol{\varepsilon}) \end{aligned} \tag{7}$$

where $\hat{\mathbf{S}}_+$, $\hat{\mathbf{S}}_-$ are the atomic raising and lowering operators, respectively:

$$\hat{\mathbf{S}}_+ = \sum_{m_g=-J_g}^{J_g} \sum_{q=0,\pm1} \langle J_g, m_g, 1, q | J_e, m_g + q\rangle (\hat{\mathbf{e}}_q^z)^* |e_{m_g+q}\rangle\langle g_{m_g}|$$

and $\hat{\mathbf{S}}_- = (\hat{\mathbf{S}}_+)^\dagger$.

In our work, we use the Wigner representation of the atomic density matrix which is most suited for the study

of the atomic motion in the semi-classical limit. In this representation, the density operator $\hat{\rho}$ is represented by the Wigner matrix $\boldsymbol{W}(\mathbf{r},\mathbf{p},t)$:

$$\boldsymbol{W}(\mathbf{r},\mathbf{p},t)=\frac{1}{h^3}\int \mathrm{d}^3u\langle \mathbf{r}+\frac{1}{2}\mathbf{u}|\hat{\rho}(t)|\mathbf{r}-\frac{1}{2}\mathbf{u}\rangle \mathrm{e}^{-\mathrm{i}\mathbf{p}\cdot\mathbf{u}/\hbar}. \quad (8)$$

And we also define the Wigner function $R(\mathbf{r},\mathbf{p},t)$ being the trace of $\boldsymbol{W}$:

$$R(\mathbf{r},\mathbf{p},t)=\mathrm{Tr}\left(\boldsymbol{W}(\mathbf{r},\mathbf{p},t)\right). \quad (9)$$

From equations (6, 8), we obtain the equation of motion for $\boldsymbol{W}(\mathbf{r},\mathbf{p},t)$:

$$\begin{aligned}\frac{\partial}{\partial t}\boldsymbol{W}(\mathbf{r},\mathbf{p},t)=&-\mathbf{v}\cdot\boldsymbol{\nabla}\boldsymbol{W}(\mathbf{r},\mathbf{p},t)\\&+\frac{1}{\mathrm{i}\hbar}[\hat{H}_{\mathrm{Ai}},\boldsymbol{W}(\mathbf{r},\mathbf{p},t)]+S(\boldsymbol{W}(\mathbf{r},\mathbf{p},t))\\&-\int \mathrm{d}^3\kappa\frac{\mathrm{e}^{\mathrm{i}\boldsymbol{\kappa}\cdot\mathbf{r}}}{\mathrm{i}\hbar}\Big[\boldsymbol{W}(\mathbf{r},\mathbf{p}+\frac{1}{2}\hbar\boldsymbol{\kappa},t)\hat{\mathcal{H}}_{\mathrm{A-L}}(\boldsymbol{\kappa})\\&-\hat{\mathcal{H}}_{\mathrm{A-L}}(\boldsymbol{\kappa})\boldsymbol{W}(\mathbf{r},\mathbf{p}-\frac{1}{2}\hbar\boldsymbol{\kappa},t)\Big] \quad (10)\end{aligned}$$

where $\mathbf{v}=\mathbf{p}/m$ is the atomic velocity, $\hat{H}_{\mathrm{Ai}}=\hat{H}_{\mathrm{A}}-\hat{P}^2/2m$ and $\hat{\mathcal{H}}_{\mathrm{A-L}}(\boldsymbol{\kappa})$ is the Fourier transform of $\hat{H}_{\mathrm{A-L}}(\mathbf{r})$: $\hat{\mathcal{H}}_{\mathrm{A-L}}(\boldsymbol{\kappa})=\int \mathrm{d}^3r\ \mathrm{e}^{-\mathrm{i}\boldsymbol{\kappa}\cdot\mathbf{r}}\hat{H}_{\mathrm{A-L}}(\mathbf{r})$.

In the semi-classical limit stated in the beginning of this section, we can apply Bogolyubov's procedure to reduce equation (10) into a kinetic equation for the Wigner function $R(\mathbf{r},\mathbf{p},t)$ [18,19]. First, let us expand $\boldsymbol{W}(\mathbf{r},\mathbf{p}+\frac{1}{2}\hbar\boldsymbol{\kappa},t)$ as:

$$\begin{aligned}\boldsymbol{W}(\mathbf{r},\mathbf{p}\pm\frac{1}{2}\hbar\boldsymbol{\kappa},t)=&\boldsymbol{W}(\mathbf{r},\mathbf{p},t)\pm\frac{1}{2}\hbar\boldsymbol{\kappa}\cdot\frac{\partial}{\partial\mathbf{p}}\boldsymbol{W}(\mathbf{r},\mathbf{p},t)\\&+\frac{\hbar^2}{2}\sum_{i,j}\frac{1}{2}\kappa_i\frac{1}{2}\kappa_j\frac{\partial^2}{\partial p_i\partial p_j}\boldsymbol{W}(\mathbf{r},\mathbf{p},t)+\cdots\end{aligned}$$

Putting the above equation into (10), we get:

$$\left(\frac{\partial}{\partial t}+\mathbf{v}\cdot\boldsymbol{\nabla}\right)\boldsymbol{W}(\mathbf{r},\mathbf{p},t)=(\mathrm{Ł}_{\mathrm{Bloch}}+\mathrm{Ł}_1+\mathrm{Ł}_2)\boldsymbol{W}(\mathbf{r},\mathbf{p},t). \quad (11)$$

The explicit expressions for operators $\mathrm{Ł}_{\mathrm{Bloch}}$, $\mathrm{Ł}_1$ and $\mathrm{Ł}_2$ are given in the Appendix. Next, we expand $\boldsymbol{W}(\mathbf{r},\mathbf{p},t)$ up to the first order in $\hbar k$:

$$\boldsymbol{W}=\boldsymbol{W}^{\mathrm{s}}R+\hbar k\sum_{i=x,y,z}\boldsymbol{W}_i^1\frac{\partial R}{\partial p_i}. \quad (12)$$

Substituting (12) into (11), and taking the trace, we obtain the Fokker-Planck equation for the Wigner function $R(\mathbf{r},\mathbf{p},t)$:

$$\begin{aligned}\left(\frac{\partial}{\partial t}+\mathbf{v}\cdot\boldsymbol{\nabla}\right)R=&-\frac{\partial}{\partial\mathbf{p}}(\mathbf{F}R)+\sum_{i,j}\frac{\partial}{\partial p_i}\left(D_{ij}^{\mathrm{st}}\frac{\partial R}{\partial p_j}\right)\\&+\sum_{i,j}\frac{\partial^2}{\partial p_i\partial p_j}(D_{ij}^{\mathrm{sp}}R) \quad (13)\end{aligned}$$

and the equation for the zeroth- and first-order Wigner density matrix $\boldsymbol{W}^{\mathrm{s}}$ and $\boldsymbol{W}_i^1$:

$$\mathbf{v}\cdot\boldsymbol{\nabla}\boldsymbol{W}^{\mathrm{s}}=\mathrm{Ł}_{\mathrm{Bloch}}\cdot\boldsymbol{W}^{\mathrm{s}} \quad (14)$$

$$\begin{aligned}\mathbf{v}\cdot\boldsymbol{\nabla}\boldsymbol{W}_i^1=&\mathrm{Ł}_{\mathrm{Bloch}}\cdot\boldsymbol{W}_i^1+\frac{1}{2\hbar k}[\boldsymbol{W}^{\mathrm{s}}\frac{\partial\hat{H}_{\mathrm{A-L}}}{\partial r_i}+\frac{\partial\hat{H}_{\mathrm{A-L}}}{\partial r_i}\boldsymbol{W}^{\mathrm{s}}]\\&+\frac{F_i}{\hbar k}\boldsymbol{W}^{\mathrm{s}} \quad (15)\end{aligned}$$

where

$$\mathbf{F}(\mathbf{r},\mathbf{v})=\mathrm{Tr}\left(\boldsymbol{\nabla}\hat{H}_{\mathrm{A-L}}(\mathbf{r})\boldsymbol{W}^{\mathrm{s}}\right) \quad (16)$$

is the light pressure force exerted on the atom and the coefficients D_{ij}^{st} and D_{ij}^{sp} correspond to two parts of the momentum diffusion tensor. They determine the momentum distribution broadening due to fluctuations in the number of scattered photons under stimulated and spontaneous emission, respectively:

$$D_{ij}^{\mathrm{st}}=\hbar k\,\mathrm{Tr}\left(\frac{\partial\hat{H}_{\mathrm{A-L}}}{\partial r_i}\boldsymbol{W}_j^1\right) \quad (17)$$

$$\begin{aligned}D_{ij}^{\mathrm{sp}}=&\frac{1}{2}\hbar^2k^2\Gamma\\&\times\mathrm{Tr}\left(\int\frac{\mathrm{d}^2\kappa}{8\pi/3}\kappa_i\kappa_j\sum_{\boldsymbol{\varepsilon}\perp\boldsymbol{\kappa}}(\hat{\mathbf{S}}_-\cdot\boldsymbol{\varepsilon}^*)\boldsymbol{W}^{\mathrm{s}}(\hat{\mathbf{S}}_+\cdot\boldsymbol{\varepsilon})\right). \quad (18)\end{aligned}$$

By solving equations (14, 15), we obtain $\boldsymbol{W}^{\mathrm{s}}$ and $\boldsymbol{W}_i^1$. And hence we can calculate the light pressure force and the momentum diffusion tensors, from which the atomic Wigner function can be calculated by integrating the Fokker-Planck equation (13). Next, as an example, we will apply the theory outlined above to study an atom with $J_{\mathrm{g}}=1\leftrightarrow J_{\mathrm{e}}=1$ transition interacting with a 2D light field with $\sigma^+-\sigma^-$ configuration.

3 Typical results: A study of a $1\leftrightarrow 1$ transition

The atomic energy levels and the laser fields under consideration are schematically shown in Figure 1. In the absence of the magnetic field, this system has been shown to reach temperatures below the single-photon recoil limit *via* velocity selective coherent population trapping (VSCPT) [16].

The electric field shown in Figure 1b can be written as:

$$\begin{aligned}\mathbf{E}(\mathbf{r})=&[E_1(\mathrm{e}^{\mathrm{i}kx}\hat{\mathbf{e}}_x^+ +\mathrm{e}^{-\mathrm{i}kx}\hat{\mathbf{e}}_x^-)\mathrm{e}^{-\mathrm{i}\omega_{\mathrm{L}}t}+cc]\\&+[E_2\mathrm{e}^{\mathrm{i}\varphi}(\mathrm{e}^{\mathrm{i}ky}\hat{\mathbf{e}}_y^+ +\mathrm{e}^{-\mathrm{i}ky}\hat{\mathbf{e}}_y^-)\mathrm{e}^{-\mathrm{i}\omega_{\mathrm{L}}t}+cc] \quad (19)\end{aligned}$$

where $\hat{\mathbf{e}}_\pm^x=\mp(\hat{\mathbf{e}}_y\pm\mathrm{i}\hat{\mathbf{e}}_z)/\sqrt{2}$, and $\hat{\mathbf{e}}_\pm^y=\mp(\hat{\mathbf{e}}_z\pm\mathrm{i}\hat{\mathbf{e}}_x)/\sqrt{2}$. This can be rewritten in the general form of equation (1) as:

$$\begin{aligned}\mathbf{E}(\mathbf{r})=&\sum_{q=0,\pm}E_q(\mathbf{r})\hat{\mathbf{e}}_q^z\mathrm{e}^{-\mathrm{i}\omega_{\mathrm{L}}t}+cc,\\E_\pm(\mathbf{r})=&\ \mathrm{i}(E_1\sin kx\mp E_2\mathrm{e}^{\mathrm{i}\varphi}\cos ky),\\E_0(\mathbf{r})=&\ \sqrt{2}(E_1\cos kx+E_2\mathrm{e}^{\mathrm{i}\varphi}\sin ky). \quad (20)\end{aligned}$$

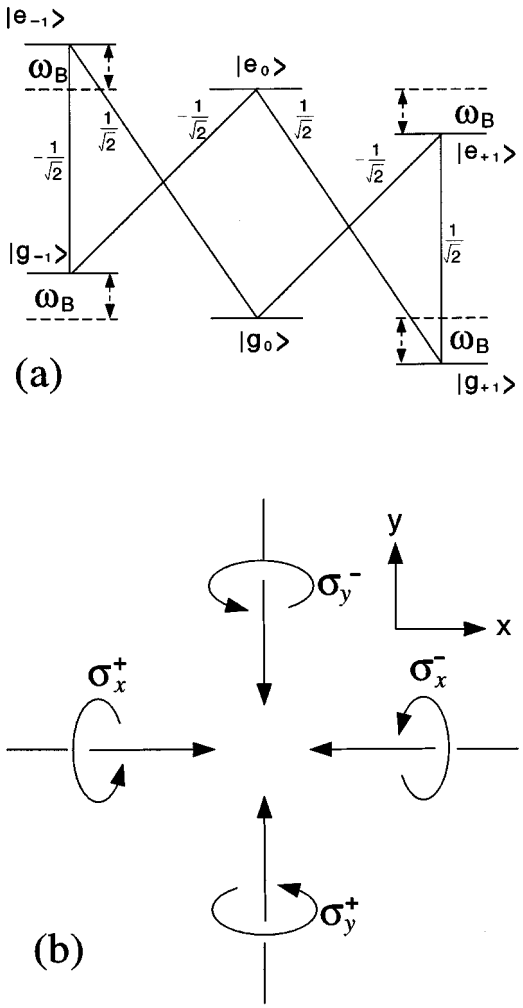

Fig. 1. (a) Atomic energy levels for a $J_g = 1 \leftrightarrow J_e = 1$ transition. The Clebsch-Gordan coefficients are also show in the figure. (b) 2D $\sigma^+ - \sigma^-$ laser configuration.

3.1 Velocity-dependent light pressure force

Figure 2 illustrates the typical character of the light pressure force as a function of velocity. Since we are most interested in the atomic momentum distribution, we have spatially averaged the force over the periodicity of the light field. Furthermore, we can decompose the force into a spontaneous part, $\mathbf{F}_{\rm sp}$, and a stimulated part, $\mathbf{F}_{\rm st}$. The spontaneous force can be understood as a consequence of the momentum transferred to the atom from the absorption-spontaneous emission cycles, while the stimulated force arises from the interaction between the in-phase component of the atomic dipole moment induced by the light field and the gradient of the field itself.

As shown in Figure 2, the spontaneous force itself has two components: a spontaneous anisotropic force, $\mathbf{F}_{\rm sp\_ani}$, and a velocity space vortical force, $\mathbf{F}_{\rm sp\_vort}$. $\mathbf{F}_{\rm sp\_ani}$ is similar to the anisotropic force in the case of two-level atoms [14]. It heats the atom along one axis while cools it along the orthogonal axis. $\mathbf{F}_{\rm sp\_vort}$ arises from the presence of the magnetic field and changes sign once the direction of the magnetic field is reversed.

The property of the spontaneous vortical force, $\mathbf{F}_{\rm sp\_vort}$, is reminiscent of a charged particle moving in a magnetic field. In fact, in the low velocity region, this force can be fit to a "Lorentz" force:

$$\mathbf{F}_{\rm sp\_vort} = Q_{\rm eff}\mathbf{v} \times \mathbf{B} \tag{21}$$

where $Q_{\rm eff}$ can be regarded as an *effective charge* induced by the laser-atom interaction. For the case show in Figure 2, we estimate that $Q_{\rm eff} \approx -5.4 \times 10^{-19}$ coulomb or 3.4 electrons for the $2^3S_1 \leftrightarrow 2^3P_1$ transition of metastable ^{4}He*. $Q_{\rm eff}$ changes sign as Δ changes sign, and vanishes at $\Delta = 0$.

The stimulated force also contains two parts: an isotropic part, $\mathbf{F}_{\rm st\_iso}$, and an anisotropic part, $\mathbf{F}_{\rm st\_ani}$. Like $\mathbf{F}_{\rm sp\_vort}$, $\mathbf{F}_{\rm st\_ani}$ also vanishes in the absence of the magnetic field. For the case shown in Figure 2, $\mathbf{F}_{\rm st\_ani}$ is a heating force along $(\hat{\mathbf{e}}_x - \hat{\mathbf{e}}_y)$ and a cooling force along the perpendicular direction $(\hat{\mathbf{e}}_x + \hat{\mathbf{e}}_y)$. $\mathbf{F}_{\rm st\_iso}$ vanishes at $\Delta = 0$, while $\mathbf{F}_{\rm st\_ani}$ doesn't.

Analytical expressions for the forces can be obtained under the appropriate limits of low field intensity, low atomic velocity and large magnetic field. Under these limits, we can neglect the excited states population and coherences $\rho_{\rm ee}(m_e, m'_e)$, and the Zeeman coherence between different magnetic sublevels of the ground state $\rho_{\rm gg}(m_g, m'_g)$. And the ground-excited coherences, $\rho_{\rm ge}(m_g, m_e)$ and $\rho_{\rm eg}(m_e, m_g)$, follow adiabatically the ground state population. The results can be summarized in the following:

$$\begin{aligned}
&\mathbf{F}_{\rm sp_ani} \propto \sin(2\varphi)(v_x\hat{\mathbf{e}}_x - v_y\hat{\mathbf{e}}_y),\\
&\mathbf{F}_{\rm sp_vort} \propto -\Delta\omega_{\rm B}(v_y\hat{\mathbf{e}}_x - v_x\hat{\mathbf{e}}_y),\\
&\mathbf{F}_{\rm st_iso} \propto -\Delta(v_x\hat{\mathbf{e}}_x + v_y\hat{\mathbf{e}}_y),\\
&\mathbf{F}_{\rm st_ani} \propto \omega_{\rm B}\sin(2\varphi)(v_y\hat{\mathbf{e}}_x + v_x\hat{\mathbf{e}}_y).
\end{aligned}$$

3.2 Momentum space distribution

As mentioned earlier, we can apply the same continued fraction method to calculate the momentum diffusion tensor. The force and diffusion coefficients can therefore be used to solve the Fokker-Planck equation (13), and the atomic distribution in momentum space can hence be obtained. Figure 3 illustrates the steady state momentum distribution for a red-detuned laser field without the presence of magnetic field. The distribution clearly shows its dependence on the time-phase delay φ. For red-detuning, the light pressure force is a cooling force for large velocity and a heating force for small velocity. This feature arises from the interplay between the Doppler cooling force and a "Sisyphus" heating force [20]. As a result, the force becomes zero at certain non-zero critical velocities, around which the atoms will be localized in momentum space. A plot of this critical velocity as a function of Rabi frequency is shown in Figure 4. For blue-detuned laser light, the force changes sign: it becomes a heating force for large velocity and a cooling force for small velocity.

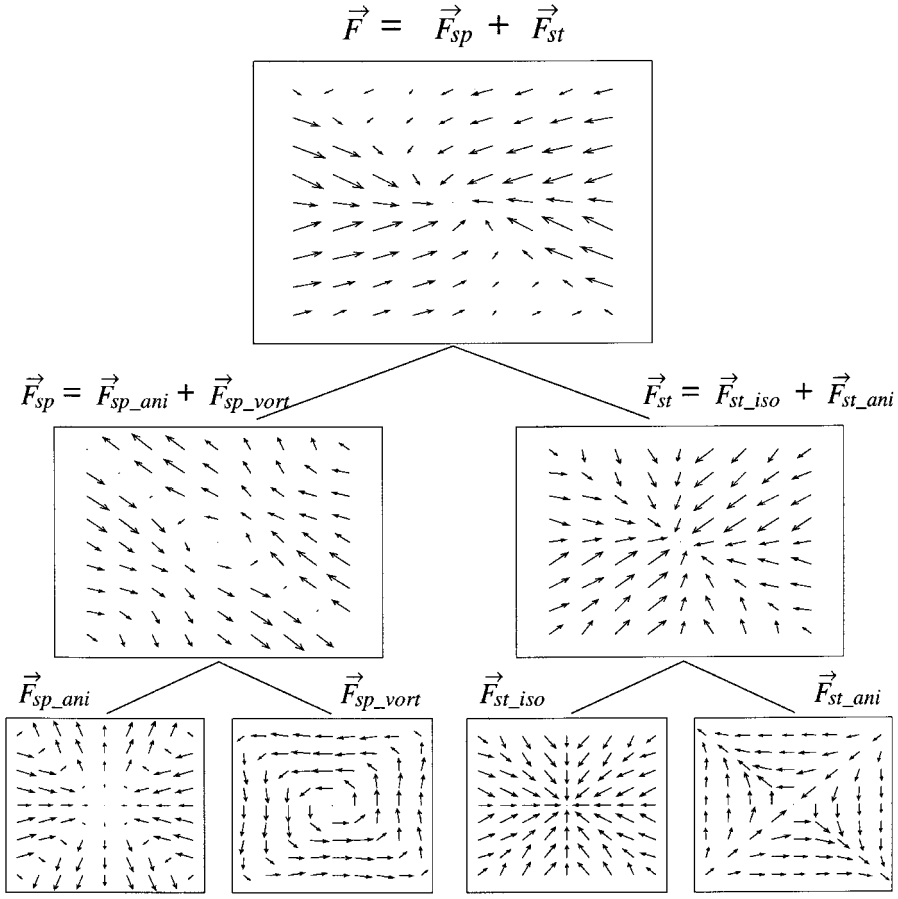

Fig. 2. Vector plots of the light pressure force. Here $g_1 = g_2 = 0.25\Gamma$ ($g_i = 2\langle e||d||g\rangle E_i/\hbar$ is the Rabi frequency), $\Delta = 0.5\Gamma$, $\omega_{\rm B} = 1.5\Gamma$ and $\varphi = 0.25\pi$. The velocity range shown in the figure is $v_{x,y} \in [-0.5, 0.5]\,\Gamma/k$. The longest arrow in the plot of total force, **F**, corresponds to a force with magnitude of $0.018\hbar k\Gamma$.

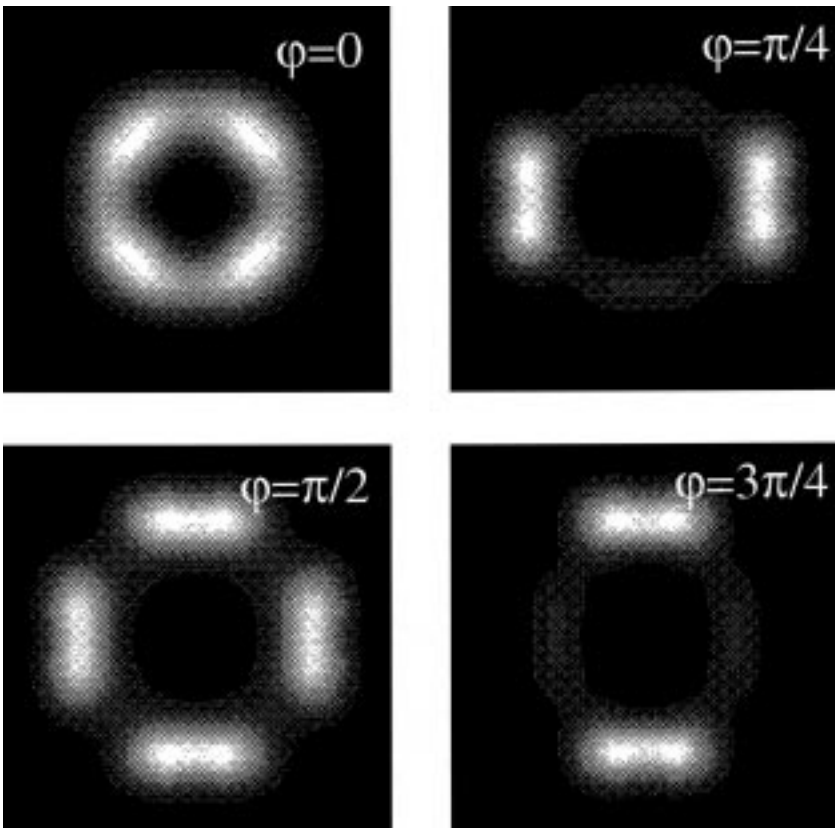

Fig. 3. Steady state momentum space distribution. Here $g_1 = g_2 = 1.8\Gamma$, $\Delta = -\Gamma$, $\omega_{\rm B} = 0$. The velocity range shown in the figure is $v_{x,y} \in [-1.5, 1.5]\,\Gamma/k$.

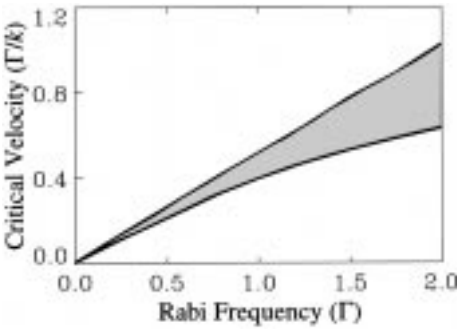

Fig. 4. Critical velocity at the axis $v_y = 0$ as a function of Rabi frequency. Here $\Delta = -\Gamma$. For a given Rabi frequency, the critical velocity falls in the shaded area depending on the time-phase delay φ.

In the 2D VSCPT experiment, it has been speculated that the blue-detuned laser light may cause a friction force at low atomic velocity, which significantly enhances the rate of population to the dark state around zero-momentum and hence the efficiency of the VSCPT process [16]. Our calculations here confirms this expectation in detail.

Our method can readily be applied to other level configurations. If we consider a $1 \leftrightarrow 2$ transition using the same field configuration, we find many features in common with the $1 \leftrightarrow 1$ transition such as the anisotropic spontaneous force, a phase dependent force and the magnetic field induced vortical force. Like the $1 \leftrightarrow 1$ transition, the $1 \leftrightarrow 2$ transition is of particular interest: the 1D case of a $1 \leftrightarrow 2$ transition in $\sigma^+ - \sigma^-$ laser field has been studied in detail in the context of sub-Doppler cooling and the idea of polarization gradient cooling process [7]. Figure 5 illustrates the 2D velocity-dependent force under similar conditions used to study sub-Doppler cooling. For red detuning, we see a cooling over the entire velocity range. Of key importance, however, is that in 2D we also we observe an enhancement in the friction coefficient at low velocity (see Fig. 5b). This feature is a clear signature of polarization gradient cooling, analogous to the 1D case [7]. As an illustration of the effect of multi-dimensionality, we show in the inset of Figure 5b the friction coefficient along x axis at low velocity as a function of time-phase delay φ. Remarkably, we do not find field parameters which give rise to the turn over in the velocity dependent force described in detail above.

4 Conclusion

In this paper, we described a general semi-classical laser cooling theory for an atom interacting with a two-dimensional laser field. We calculate the light pressure force and momentum diffusion coefficients from the optical Bloch equations and study the momentum space distribution of the atom by solving the Fokker-Planck equation. This theory applies to an arbitrary $J_g \leftrightarrow J_e$ electric dipole transition, arbitrary 2D laser field configurations, as well as arbitrary atomic velocities (within the limit of semi-classical theory, *i.e.*, the velocity of atom $\gg$ single photon recoil velocity).

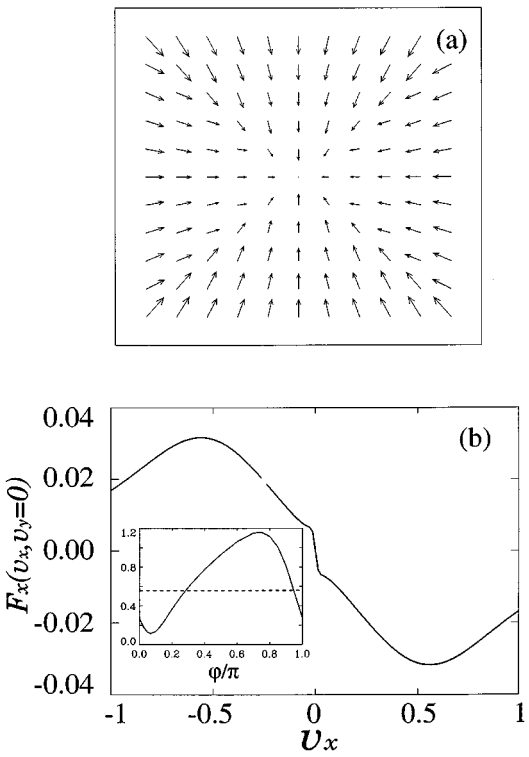

Fig. 5. (a) Vector plot of the light pressure force for a $1 \leftrightarrow 2$ transition. Here $g_1 = g_2 = 0.25\Gamma$, $\Delta = -0.5\Gamma$ and $\varphi = \pi/4$. The velocity range shown in the figure is $v_{x,y} \in [-0.5, 0.5]\ \Gamma/k$. (b) Light pressure force along axis $v_y = 0$. The units for force and velocity are $\hbar k\Gamma$ and Γ/k, respectively. Inset in (b) shows the friction coefficient (in units of $\hbar k^2$) at low velocity as a function of φ. Dashed line represents its value in 1D, obtained by taking $g_2 = 0$.

We applied this theory to study an atom with $J_g = 1 \leftrightarrow J_e = 1$ transition in a 2D $\sigma^+ - \sigma^-$ laser field. We showed that the light pressure force possesses striking new features which are unique to multi-dimensional systems. For example, in the presence of a magnetic field, there exists a vortical force as if the neutral atom were a charged particle experiencing the Lorentz force. The effective charge can be as large as several electrons. Our calculation confirms that there does exist a friction Sisyphus force in the 2D VSCPT configuration with blue-detuned laser light (as has been suggested by the experimental observations), which may significantly enhance the efficiency of the VSCPT. The results of a $1 \leftrightarrow 2$ transition was also briefly mentioned, and we did not find in this case the critical velocity at which the force changes from cooling to heating, or *vice versa*.

To solve the 2D Bloch equations, we developed a generalized matrix continued fraction method. The idea is to expand the density matrix elements into Fourier series and obtain a double-index recurrence equation. By grouping the Fourier coefficients into N-photon groups (see Appendix B), we can reduce the double-index equation

$$\mathbf{v}\cdot\boldsymbol{\nabla}W^{\rm s}_{\rm ee}(m_{\rm e},m'_{\rm e}) = [-\Gamma + {\rm i}(m_{\rm e}-m'_{\rm e})g_{\rm e}\omega_{\rm B}]W^{\rm s}_{\rm ee}(m_{\rm e},m'_{\rm e}) + \frac{\rm i}{2}\sum_{q=0,\pm1}\langle J_{\rm g},m_{\rm e}-q,1,q|J_{\rm e},m_{\rm e}\rangle g_q(\mathbf{r})W^{\rm s}_{\rm ge}(m_{\rm e}-q,m'_{\rm e}) - \frac{\rm i}{2}\sum_{q=0,\pm1}\langle J_{\rm g},m'_{\rm e}-q,1,q|J_{\rm e},m'_{\rm e}\rangle g^*_q(\mathbf{r})W^{\rm s}_{\rm eg}(m_{\rm e},m'_{\rm e}-q) \quad \text{(A.4a)}$$

$$\mathbf{v}\cdot\boldsymbol{\nabla}W^{\rm s}_{\rm eg}(m_{\rm e},m_{\rm g}) = [-\frac{1}{2}\Gamma + {\rm i}(\Delta + (g_{\rm e}m_{\rm e}-g_{\rm g}m_{\rm g})\omega_{\rm B})]W^{\rm s}_{\rm eg}(m_{\rm e},m_{\rm g}) + \frac{\rm i}{2}\sum_{q=0,\pm1}\langle J_{\rm g},m_{\rm e}-q,1,q|J_{\rm e},m_{\rm e}\rangle g_q(\mathbf{r})W^{\rm s}_{\rm gg}(m_{\rm e}-q,m_{\rm g}) - \frac{\rm i}{2}\sum_{q=0,\pm1}\langle J_{\rm g},m_{\rm g},1,q|J_{\rm e},m_{\rm g}+q\rangle g_q(\mathbf{r})W^{\rm s}_{\rm ee}(m_{\rm e},m_{\rm g}+q) \quad \text{(A.4b)}$$

$$\mathbf{v}\cdot\boldsymbol{\nabla}W^{\rm s}_{\rm gg}(m_{\rm g},m'_{\rm g}) = {\rm i}(m_{\rm g}-m'_{\rm g})g_{\rm g}\omega_{\rm B}W^{\rm s}_{\rm gg}(m_{\rm g},m'_{\rm g}) + \Gamma\sum_{q=0,\pm1}\langle J_{\rm g},m_{\rm g},1,q|J_{\rm e},m_{\rm g}+q\rangle\langle J_{\rm g},m'_{\rm g},1,q|J_{\rm e},m'_{\rm g}+q\rangle W^{\rm s}_{\rm ee}(m_{\rm g}+q,m'_{\rm g}+q) + \frac{\rm i}{2}\sum_{q=0,\pm1}\langle J_{\rm g},m_{\rm g},1,q|J_{\rm e},m_{\rm g}+q\rangle g^*_q(\mathbf{r})W^{\rm s}_{\rm eg}(m_{\rm g}+q,m'_{\rm g}) - \frac{\rm i}{2}\sum_{q=0,\pm1}\langle J_{\rm g},m'_{\rm g},1,q|J_{\rm e},m'_{\rm g}+q\rangle g_q(\mathbf{r})W^{\rm s}_{\rm ge}(m_{\rm g},m'_g+q) \quad \text{(A.4c)}$$

into a single-index equation which has been studied before using a continued fraction method. This technique is very efficient and reduces computing time enormously compared with the usual integration method [11]. It provides us with a powerful tool to investigate complex dependences of the light pressure force, momentum diffusion coefficients and atomic motion on laser/atom parameters.

1D laser cooling theory has given us many insights on laser-atom interaction. However, the success of 1D theory in describing many experimental results should not obscure the fact that it does not represent the real 3D world, and therefore, that it cannot give a full description of all experimental findings. Indeed, as we have shown in this paper, there are unique features that arise from the multi-dimensionality. To develop a 3D theory is perhaps one of the most important goals in laser cooling and trapping. Our 2D theory presented here should be an important step towards this goal.

This work was supported by the National Science Foundation and by the David and Lucile Packard Foundation.

Appendix A: The optical Bloch equations for the Wigner density matrix

The explicit expressions for the operators in equation (11) are:

$$\text{Ł}_{\rm Bloch}(\mathbf{r})\cdot\boldsymbol{W}(\mathbf{r},\mathbf{p},t) = \frac{1}{{\rm i}\hbar}[\hat{H}_{\rm Ai}+\hat{H}_{\rm A-L}(\mathbf{r}),\boldsymbol{W}(\mathbf{r},\mathbf{p},t)] - \frac{1}{2}\Gamma[(\hat{\mathbf{S}}_+\cdot\hat{\mathbf{S}}_-)\boldsymbol{W}(\mathbf{r},\mathbf{p},t) + \boldsymbol{W}(\mathbf{r},\mathbf{p},t)(\hat{\mathbf{S}}_+\cdot\hat{\mathbf{S}}_-)] + \Gamma\int\frac{{\rm d}^2\kappa}{8\pi/3}\sum_{\boldsymbol{\varepsilon}\perp\boldsymbol{\kappa}}(\hat{\mathbf{S}}_-\cdot\boldsymbol{\varepsilon}^*)\boldsymbol{W}(\mathbf{r},\mathbf{p},t)(\hat{\mathbf{S}}_+\cdot\boldsymbol{\varepsilon}), \quad \text{(A.1)}$$

$$\text{Ł}_1(\mathbf{r},\mathbf{p},t)\cdot\boldsymbol{W}(\mathbf{r},\mathbf{p},t) = \frac{1}{2}\left[\frac{\partial\boldsymbol{W}}{\partial\mathbf{p}}\cdot\frac{\partial\hat{H}_{\rm A-L}}{\partial\mathbf{r}} + \frac{\partial\hat{H}_{\rm A-L}}{\partial\mathbf{r}}\cdot\frac{\partial\boldsymbol{W}}{\partial\mathbf{p}}\right], \quad \text{(A.2)}$$

$$\text{Ł}_2(\mathbf{r},\mathbf{p},t)\cdot\boldsymbol{W}(\mathbf{r},\mathbf{p},t) = -\frac{{\rm i}\hbar}{8}\sum_{i,j}\left[\frac{\partial^2\boldsymbol{W}}{\partial p_i\partial p_j},\frac{\partial^2}{\partial r_i\partial r_j}\hat{H}_{\rm A-L}\right] + \frac{\hbar^2k^2\Gamma}{2}\sum_{i,j}\int\frac{{\rm d}^2\kappa}{8\pi/3}\kappa_i\kappa_j\sum_{\boldsymbol{\varepsilon}\perp\boldsymbol{\kappa}}(\hat{\mathbf{S}}_-\cdot\boldsymbol{\varepsilon}^*)\frac{\partial^2\boldsymbol{W}}{\partial p_i\partial p_j}(\mathbf{S}_+\cdot\boldsymbol{\varepsilon}). \quad \text{(A.3)}$$

From equation (14), we obtain the optical Bloch equations for the zeroth order Wigner density matrix:

see equations (A.4a, A.4b, A.4c) above

where

$$W^{\rm s}_{\rm ee}(m_{\rm e},m'_{\rm e}) \equiv \langle e_{m_{\rm e}}|\boldsymbol{W}^{\rm s}(\mathbf{r},\mathbf{p},t)|e_{m'_{\rm e}}\rangle,$$

$$W^{\rm s}_{\rm eg}(m_{\rm e},m_{\rm g}) = [W^{\rm s}_{\rm ge}(m_{\rm g},m_{\rm e})]^* \equiv \langle e_{m_{\rm e}}|\mathbf{W}^{\rm s}(\mathbf{r},\mathbf{p},t)|g_{m_{\rm g}}\rangle,$$

$$W^{\rm s}_{\rm gg}(m_{\rm g},m'_{\rm g}) \equiv \langle g_{m_{\rm g}}|\mathbf{W}^{\rm s}(\mathbf{r},\mathbf{p},t)|g_{m'_g}\rangle.$$

Similar equations for the first order Wigner density matrix elements $\boldsymbol{W}^1$ can be obtained from (15).

The conservation of total population requires:

$$\sum_{m_{\rm e}=-J_{\rm e}}^{J_{\rm e}}W^{\rm s}_{\rm ee}(m_{\rm e},m_{\rm e}) + \sum_{m_{\rm g}=-J_{\rm g}}^{J_{\rm g}}W^{\rm s}_{\rm gg}(m_{\rm g},m_{\rm g}) = 1. \quad \text{(A.5)}$$

Appendix B: Two-dimensional continued fraction method

Here we describe in detail the 2D continued fraction method. First, let us expand the density matrix elements into Fourier series:

$$W^{\rm s}_{\rm ee}(m_{\rm e},m'_{\rm e})=\sum_{n,m}W^{(n,m)}_{\rm ee}(m_{\rm e},m'_{\rm e}){\rm e}^{{\rm i}nkx+{\rm i}mky}, \quad \text{(B.1a)}$$

$$W^{\rm s}_{\rm eg}(m_{\rm e},m_{\rm g})=\sum_{n,m}W^{(n,m)}_{\rm eg}(m_{\rm e},m_{\rm g}){\rm e}^{{\rm i}nkx+{\rm i}mky}, \quad \text{(B.1b)}$$

$$W^{\rm s}_{\rm ge}(m_{\rm g},m_{\rm e})=\sum_{n,m}W^{(n,m)}_{\rm ge}(m_{\rm g},m_{\rm e}){\rm e}^{{\rm i}nkx+{\rm i}mky}, \quad \text{(B.1c)}$$

$$W^{\rm s}_{\rm gg}(m_{\rm g},m'_{\rm g})=\sum_{n,m}W^{(n,m)}_{\rm gg}(m_{\rm g},m'_{\rm g}){\rm e}^{{\rm i}nkx+{\rm i}mky}. \quad \text{(B.1d)}$$

Similarly, expand the Rabi frequencies $g_q(\mathbf{r})$ as:

$$g_q(\mathbf{r})=g^+_{q\_x}{\rm e}^{{\rm i}kx}+g^-_{q\_x}{\rm e}^{-{\rm i}kx}+g^+_{q\_y}{\rm e}^{{\rm i}ky}+g^-_{q\_y}{\rm e}^{-{\rm i}ky} \quad \text{(B.2)}$$

By substituting equations (B.1, B.2) into (A.4, A.5), equating the left sides of the equations to the right sides with the same expansion order ($\mathrm{e}^{{\rm i}nkx+{\rm i}mky}$), we obtain a double-index recurrence equations for the Fourier coefficients:

$$\begin{aligned}&M(n,m)\mathbf{W}(n,m)+M^{+0}\mathbf{W}(n+1,m)\\&+M^{-0}\mathbf{W}(n-1,m)+M^{0+}\mathbf{W}(n,m+1)\\&+M^{0-}\mathbf{W}(n,m-1)=\mathbf{C}(n,m)\end{aligned} \quad \text{(B.3)}$$

where $\mathbf{W}(n,m)$ is a supervector which is composed of the Fourier coefficients of the density matrix elements,

$$\mathbf{W}(n,m)=\begin{pmatrix}W^{(n,m)}_{\rm ee}(m_{\rm e},m'_{\rm e})\\W^{(n,m)}_{\rm eg}(m_{\rm e},m_{\rm g})\\W^{(n,m)}_{\rm ge}(m_{\rm g},m_{\rm e})\\W^{(n,m)}_{\rm gg}(m_{\rm g},m'_{\rm g})\end{pmatrix} \quad \text{(B.4)}$$

where $m_{\rm e},m'_{\rm e}=-J_{\rm e},-J_{\rm e}+1,\cdots,J_{\rm e}-1,J_{\rm e}$ and $m_{\rm g},m'_{\rm g}=-J_{\rm g},-J_{\rm g}+1,\cdots,J_{\rm g}-1,J_{\rm g}$. The vector $\mathbf{W}(n,m)$ has $N_{\rm d}=(2J_{\rm e}+1+2J_{\rm g}+1)^2-1$ elements (the -1 results from the constraint of the total population as in Eq. (A.5)), and matrices $M^{\pm0}$, $M^{0\pm}$ and $M(n,m)$ are of dimensions $N_{\rm d}\times N_{\rm d}$.

Let us group those vectors $\mathbf{W}(n,m)$ with the same value of $N=|n|+|m|$ together, and call it the N-photon group. We immediately notice from equation (B.3) that the N-photon group is only coupled with the $(N\pm1)$-photon group. Now, let us construct two sets of supervectors $\mathbf{S}_N$ and $\mathbf{U}_N$ in the following:

$$\mathbf{S}_0=\mathbf{W}(0,0),\quad \mathbf{U}_0=\mathbf{C}(0,0) \quad \text{(B.5)}$$

$$\mathbf{S}_N=\begin{pmatrix}\mathbf{W}(-N+1,1)\\\mathbf{W}(-N+2,2)\\\vdots\\\mathbf{W}(0,N)\\\mathbf{W}(1,N-1)\\\vdots\\\mathbf{W}(N,0)\\\mathbf{W}(N-1,-1)\\\vdots\\\mathbf{W}(0,-N)\\\mathbf{W}(-1,-N+1)\\\vdots\\\mathbf{W}(-N,0)\end{pmatrix},$$

$$\mathbf{U}_N=\begin{pmatrix}\mathbf{C}(-N+1,1)\\\mathbf{C}(-N+2,2)\\\vdots\\\mathbf{C}(0,N)\\\mathbf{C}(1,N-1)\\\vdots\\\mathbf{C}(N,0)\\\mathbf{C}(N-1,-1)\\\vdots\\\mathbf{C}(0,-N)\\\mathbf{C}(-1,-N+1)\\\vdots\\\mathbf{C}(-N,0)\end{pmatrix},$$

for $N>0$. (B.6)

The vectors $\mathbf{S}_N$ are constructed in such a way that it contains all the elements in an N-photon group.

Next, we define matrices $\boldsymbol{M}_{N,N}, \boldsymbol{M}^{+}_{N,N+1}, \boldsymbol{M}^{-}_{N,N-1}$:

for $\quad N > 0$,

$$\boldsymbol{M}_{N,N} = \left[\begin{array}{cccccccccccc}
M(-N+1,1) & & & & & & & & & & & \\
 & \ddots & & & & & & & & & & \\
 & & M(0,N) & & & & & & & & & \\
 & & & M(1,N-1) & & & & & & & & \\
 & & & & \ddots & & & & & & & \\
 & & & & & M(N,0) & & & & & & \\
 & & & & & & M(N-1,-1) & & & & & \\
 & & & & & & & \ddots & & & & \\
 & & & & & & & & M(0,-N) & & & \\
 & & & & & & & & & M(-1,-N+1) & & \\
 & & & & & & & & & & \ddots & \\
 & & & & & & & & & & & M(-N,0)
\end{array}\right]
\begin{array}{l} 1 \\ \vdots \\ N \\ N+1 \\ \vdots \\ 2N \\ 2N+1 \\ \vdots \\ 3N \\ 3N+1 \\ \vdots \\ 4N \end{array}$$

$$\boldsymbol{M}^{+}_{N,N+1} = \left[\begin{array}{ccccccccccccccccc}
M^{-0} & M^{0+} & 0 & & & & & & & & & & & & & & \\
0 & M^{-0} & M^{-0} & 0 & & & & & & & & & & & & & \\
 & \ddots & \ddots & \ddots & \ddots & & & & & & & & & & & & \\
 & & 0 & M^{-0} & M^{0+} & M^{+0} & 0 & & & & & & & & & & \\
 & & & 0 & 0 & M^{0+} & M^{+0} & 0 & & & & & & & & & \\
 & & & & \ddots & \ddots & \ddots & \ddots & & & & & & & & & \\
 & & & & & & 0 & M^{0+} & M^{+0} & M^{0-} & 0 & & & & & & \\
 & & & & & & & 0 & 0 & M^{+0} & M^{0-} & 0 & & & & & \\
 & & & & & & & & \ddots & \ddots & \ddots & \ddots & & & & & \\
 & & & & & & & & & & 0 & M^{+0} & M^{0-} & M^{-0} & 0 & & \\
 & & & & & & & & & & & 0 & 0 & M^{0-} & M^{-0} & 0 & \\
 & & & & & & & & & & & & \ddots & \ddots & \ddots & \ddots & 0 \\
M^{0+} & & & & & & & & & & & & & 0 & 0 & M^{0-} & M^{-0}
\end{array}\right]
\begin{array}{l} 1 \\ 2 \\ \vdots \\ N \\ N+1 \\ \vdots \\ 2N \\ 2N+1 \\ \vdots \\ 3N \\ 3N+1 \\ \vdots \\ 4N \end{array}$$

for $\; N > 1$,

$$\boldsymbol{M}^{-}_{N,N-1} = \left[\begin{array}{cccccccccccccc}
M^{+0} & 0 & & & & & & & & & & & & M^{0-} \\
M^{0-} & M^{+0} & 0 & & & & & & & & & & & \\
0 & M^{0-} & M^{+0} & 0 & & & & & & & & & & \\
 & \ddots & \ddots & \ddots & \ddots & & & & & & & & & \\
 & & 0 & M^{0-} & M^{+0} & 0 & & & & & & & & \\
 & & & 0 & M^{0-} & 0 & 0 & & & & & & & \\
 & & & 0 & M^{-0} & M^{0-} & 0 & & & & & & & \\
 & & & & \ddots & \ddots & \ddots & \ddots & & & & & & \\
 & & & & & 0 & M^{-0} & M^{0-} & 0 & & & & & \\
 & & & & & & 0 & M^{-0} & 0 & 0 & & & & \\
 & & & & & & 0 & M^{0+} & M^{-0} & 0 & & & & \\
 & & & & & & & \ddots & \ddots & \ddots & \ddots & & & \\
 & & & & & & & & 0 & M^{0+} & M^{-0} & 0 & & \\
 & & & & & & & & & 0 & M^{0+} & 0 & 0 & \\
 & & & & & & & & & 0 & M^{+0} & M^{0+} & 0 & \\
 & & & & & & & & & & \ddots & \ddots & \ddots & 0 \\
 & & & & & & & & & & & 0 & M^{+0} & M^{0+} \\
 & & & & & & & & & & & & 0 & M^{+0}
\end{array}\right]
\begin{array}{l} 1 \\ 2 \\ 3 \\ \vdots \\ N-1 \\ N \\ N+1 \\ \vdots \\ 2N-1 \\ 2N \\ 2N+1 \\ \vdots \\ 3N-1 \\ 3N \\ 3N+1 \\ \vdots \\ 4N-1 \\ 4N \end{array}$$

and

$$\begin{aligned}
&\boldsymbol{M}_{0,0} = M(0,0), \\
&\boldsymbol{M}^{+}_{0,1} = \left[M^{0+} \;\; M^{+0} \;\; M^{0-} \;\; M^{-0}\right], \\
&\boldsymbol{M}^{-}_{1,0} = \left[M^{0-} \;\; M^{-0} \;\; M^{0+} \;\; M^{+0}\right]^{\mathrm{T}}.
\end{aligned}$$

With all the above definitions, the double-index recurrence equation (B.3) can be rewritten as single-index recurrence equations:

$$\boldsymbol{M}^{+}_{0,1}\cdot \mathbf{S}_1 + \boldsymbol{M}_{0,0}\cdot \mathbf{S}_0 \;=\; \mathbf{U}_0, \tag{B.7a}$$

$$\boldsymbol{M}^{+}_{N,N+1}\cdot \mathbf{S}_{N+1} + \boldsymbol{M}_{N,N}\cdot \mathbf{S}_N + \boldsymbol{M}^{-}_{N,N-1}\cdot \mathbf{S}_{N-1} = \mathbf{U}_N, \quad \text{for } N \geq 1. \tag{B.7b}$$

The single-index recurrence equations can be solved using the continued fraction method as has been done

in calculations of 1D velocity-dependent forces [15]. We outline the solution to equations (B.7) in the following.

Let us define:

$$\mathbf{S}_N = -\boldsymbol{Q}_N \cdot \boldsymbol{M}^-_{N,N-1} \cdot \mathbf{S}_{N-1} + \mathbf{S}^0_N, \quad N \geq 1. \text{ (B.8)}$$

Substituting the above equation into equation (B.7b), we obtain the recurrence relationships for matrices $\boldsymbol{Q}_N$ and vectors $\mathbf{S}^0_N$,

$$\boldsymbol{Q}_N = \frac{1}{\boldsymbol{M}_{N,N} + \boldsymbol{M}^+_{N,N+1} \cdot \boldsymbol{Q}_{N+1,N+1}(-\boldsymbol{Q}^-_{N+1,N})}, \quad N \geq 0; \quad \text{(B.9a)}$$

$$\mathbf{S}^0_N = \boldsymbol{Q}_N \, (\mathbf{U}_N - \boldsymbol{M}^+_{N,N+1} \cdot \mathbf{S}^0_{N+1}), \quad N \geq 1. \quad \text{(B.9b)}$$

Equations (B.9) can be rewritten in the continued fraction form:

$$\boldsymbol{Q}_N = \frac{1}{\boldsymbol{M}_{N,N} + \boldsymbol{M}^+_{N,N+1} \cdot \dfrac{1}{\boldsymbol{M}_{N+1,N+1} + \cdots} \cdot (-\boldsymbol{M}^-_{N+1,N})}$$

$$\mathbf{S}^0_N = \boldsymbol{Q}_N \cdot (\mathbf{U}_N - \boldsymbol{M}^+_{N,N+1} \cdot \boldsymbol{Q}_{N+1} \cdot (\mathbf{U}_{N+1} - \boldsymbol{M}^+_{N+1,N+2} \cdot \boldsymbol{Q}_{N+2} \cdot (\mathbf{U}_{N+2} - \boldsymbol{M}^+_{N+2,N+3} \cdots$$

And $\mathbf{S}_N$ can be solved as:

$$\begin{aligned}
\mathbf{S}_0 &= \boldsymbol{Q}_0 \cdot (\mathbf{U}_0 - \boldsymbol{M}^+_{0,1} \cdot \mathbf{S}^0_1), \\
\mathbf{S}_1 &= -\boldsymbol{Q}_1 \cdot \boldsymbol{M}^-_{1,0} \cdot \mathbf{S}_0 + \mathbf{S}^0_1, \\
\mathbf{S}_2 &= -\mathbf{Q}_2 \cdot \mathbf{M}^-_{2,1} \cdot \mathbf{S}_1 + \mathbf{S}^0_2, \\
&\vdots \\
\mathbf{S}_N &= -\mathbf{Q}_N \cdot \boldsymbol{M}^-_{N,N-1} \cdot \mathbf{S}_{N-1} + \mathbf{S}^0_N.
\end{aligned}$$

The 2D continued fraction method can be straightforwardly generalized to 3D. In 3D, we will encounter a triple-index recurrence equation which can also be reduced to a single-index recurrence equation using the same technique described here. However, the matrix size become considerably larger in 3D. An N-photon group supervector $\mathbf{S}_N$ in 2D contains $4N \times N_\mathrm{d}$ elements, while it contains $(4N^2 - 4N + 6) \times N_\mathrm{d}$ elements in 3D. For a $1 \leftrightarrow 1$ transition, $\mathbf{S}_5$ has 700 and 3010 elements in 2D and 3D, respectively. Hence the calculation in 3D becomes very time-consuming and can be impractical. However, using this method, one should be able to make a 3D calculation in the week field limit, in which case the excited state components of the density matrix can be neglected and hence the matrix size can be reduced significantly.

References

1. T. Hänsch, A. Schawlow, Opt. Commun. **13**, 68 (1975).
2. D. Wineland, H. Dehmelt, Bull. Am. Phys. Soc. **20**, 637 (1975).
3. V. Letokhov, V. Minogin, Phys. Rep. **73**, 1 (1981); A.P. Kazantsev *et al.*, J. Phys. France **42**, 1231 (1981); S. Stenholm, Rev. Mod. Phys. **58**, 699 (1986).
4. J. Gordan, A. Ashkin, Phys. Rev. A **21**, 1606 (1980).
5. S. Chu *et al.*, Phys. Rev. Lett. **55**, 48 (1985).
6. P. Lett *et al.*, Phys. Rev. Lett. **61**, 169 (1988).
7. J. Dalibard, C. Cohen-Tannoudji, J. Opt. Soc. Am. B **6**, 2023 (1989).
8. P.J. Ungar *et al.*, J. Opt. Soc. Am. B **6**, 2058 (1989).
9. A.P. Kazantsev, I.V. Krasnov, J. Opt. Soc. B **6**, 2140 (1989).
10. A. Hemmerich, T.W. Hänsch, Phys. Rev. Lett. **68**, 1492 (1992); A. Hemmerich *et al.*, Eur. Phys. Lett. **21**, 445 (1993).
11. K. Mølmer *et al.*, J. Phys. B **24**, 2327 (1991); Phys. Rev. A **44**, 5820 (1991); Laser Phys. **4**, 872 (1994).
12. V. Finkelstein *et al.*, Phys. Rev. A **46**, 7108 (1992).
13. Y. Castin *et al.*, Phys. Rev. A **50**, 5092 (1994).
14. T. Cai, N.P. Bigelow, Opt. Lett. **19**, 1768 (1994); N.P. Bigelow *et al.*, Acta Phys. Pol. A **86**, 29 (1994).
15. A. Valli, S. Stengolm, Phys. Lett. A **64**, 447 (1978); T. Cai, N.P. Bigelow, Opt. Commun. **104**, 175 (1993).
16. J. Lawall *et al.*, Phys. Rev. Lett. **73**, 1915 (1994).
17. C. Cohen-Tannoudji, in *Frontiers in Laser Spectroscopy*, Les Houches, Session XXVII, edited by R. Balian, S. Haroche, S. Lieberman (North-Holland, Amsterdam, 1977), Vol. 1.
18. N.N. Bogolyubov, *Lectures on Quantum Statistics* (Gordon and Breach, New York, 1967), Vol. 1; R.L. Liboff, *Introduction to the Theory of Kinetic Equations* (Wiley, New York, 1969).
19. T. Cai, Ph.D. thesis, University of Rochester, 1996.
20. J. Dalibard, C. Cohen-Tannoudji, J. Opt. Soc. Am. B **2**, 1707 (1985).